Received: 1 October 2019 | Revised: 30 October 2019 | Accepted: 4 November 2019

DOI: 10.1096/fj.201902508R

RESEARCH ARTICLE

THE FASEB JOURNAL

SAMHD1-deficient fibroblasts from Aicardi-Goutières Syndrome patients can escape senescence and accumulate mutations

Elisa Franzolin[1] | Sara Coletta[1] | Paola Ferraro[1] | Giovanna Pontarin[1] | Giulia D'Aronco[1] | Martina Stevanoni[1] | Elisa Palumbo[2] | Stefano Cagnin[1,3,4] | Loris Bertoldi[1] | Erika Feltrin[1] | Giorgio Valle[1] | Antonella Russo[2] | Vera Bianchi[1] | Chiara Rampazzo[1]

[1]Department of Biology, University of Padova, Padova, Italy

[2]Department of Molecular Medicine, University of Padova, Padova, Italy

[3]CRIBI Biotechnology Center, University of Padova, Padova, Italy

[4]CIR-Myo Myology Center, University of Padova, Padova, Italy

Correspondence
Chiara Rampazzo, Department of Biology, University of Padova, Padova, Italy.
Email: chiara.rampazzo.1@unipd.it

Funding information
This work was supported by Fondazione Telethon (project GGP14005 to V.B), Associazione Italiana per la ricerca sul cancro (AIRC project IG15818 to VB) Dipartimento di Biologia-BIRD2018 (Università di Padova) to CR

Abstract

In mammalian cells, the catabolic activity of the dNTP triphosphohydrolase SAMHD1 sets the balance and concentration of the four dNTPs. Deficiency of SAMHD1 leads to unequally increased pools and marked dNTP imbalance. Imbalanced dNTP pools increase mutation frequency in cancer cells, but it is not known if the SAMHD1-induced dNTP imbalance favors accumulation of somatic mutations in non-transformed cells. Here, we have investigated how fibroblasts from Aicardi-Goutières Syndrome (AGS) patients with mutated SAMHD1 react to the constitutive pool imbalance characterized by a huge dGTP pool. We focused on the effects on dNTP pools, cell cycle progression, dynamics and fidelity of DNA replication, and efficiency of UV-induced DNA repair. AGS fibroblasts entered senescence prematurely or upregulated genes involved in G1/S transition and DNA replication. The normally growing AGS cells exhibited unchanged DNA replication dynamics and, when quiescent, faster rate of excision repair of UV-induced DNA damages. To investigate whether the lack of SAMHD1 affects DNA replication fidelity, we compared de novo mutations in AGS and WT cells by exome next-generation sequencing. Somatic variant analysis indicated a mutator phenotype suggesting that SAMHD1 is a caretaker gene whose deficiency is per se mutagenic, promoting genome instability in non-transformed cells.

KEYWORDS

deoxynucleotide catabolism, deoxynucleotide pool imbalance, sterile alpha motif and HD domain containing protein 1 (SAMHD1), UV-induced DNA repair

Abbreviations: 6-4PPs, 6-4 pyrimidone photoproducts; ADA, adenosine deaminase; AGS, Aicardi-Goutières Syndrome; APH, aphidicolin; BRCA1, breast cancer 1; CDC7, Cell Division Cycle 7; CDT1, chromatin licensing and DNA replication factor 1; CPDs, cyclobutane pyrimidine dimers; dATP, deoxyadenosine triphosphate; dCTP, deoxycytidine triphosphate; dGTP, deoxyguanosine triphosphate; dNTP, deoxyribonucleoside triphosphate; dTTP, deoxythymidine triphosphate; E2F2, E2F Transcription Factor 2; FADU, fluorometric analysis of DNA unwinding; FCS, fetal calf serum; IOD, inter-origin distance; MLH1, MutL homolog 1; PNP, purine nucleoside phosphorylase; PRIM1, DNA primase subunit 1; RNR, ribonucleotide reductase; SAMHD1, sterile alpha motif and HD domain containing protein 1; WES, whole exome sequencing.

1 | INTRODUCTION

A critical factor for the fidelity of DNA synthesis is the availability of appropriate and balanced intracellular concentrations of deoxynucleoside triphosphates (dNTPs).[1,2] The sizes of the four dNTP pools depend on a network of synthetic and catabolic enzymes that control and adjust dNTP concentrations to the needs of DNA replication and repair and to changes in the cell microenvironment.[3,4] The onset of nuclear DNA synthesis coincides with a large expansion of dNTP pools guaranteed by S phase–specific upregulation of ribonucleotide reductase (RNR) and cytosolic thymidine kinase 1 (TK1). Following S phase, R2, the essential small subunit of RNR, and TK1 are eliminated by regulated proteolysis resulting in about 10-fold decreased concentrations of dNTPs.[5] Not only is the synthesis of dNTPs strictly regulated but also their degradation, with the deoxynucleotide triphosphohydrolase SAMHD1 as the major player. Similar to RNR, SAMHD1 is an oligomeric enzyme, allosterically regulated in both its activity and substrate specificity by (deoxy)-ribonucleoside triphosphates binding to its allosteric sites.[6,7] In contrast to RNR, SAMHD1 is a nuclear protein. We previously showed that SAMHD1 expression in normal human fibroblasts changes with their proliferation state.[8] The protein accumulates in G0/G1 and quiescent cell states, which suggested that the enzyme may exert its activity mainly outside S phase.[8] During S phase CDK-cyclin complexes phosphorylate SAMHD1 at T592 with still debated functional implications. At first, T592 phosphorylation was interpreted as a mechanism to inactivate or downregulate SAMHD1 triphosphohydrolase activity.[9] However, we recently showed that in S phase SAMHD1 is still functional and performs a significant regulatory role in the maintenance of dNTP pool balance during DNA replication.[10] Our findings agree with the recently reported participation of T592-phosphorylated SAMHD1 in protein/protein interactions at stalled replication forks, required for the ATR-CHK1 pathway and fork restart.[11] The latter function of SAMHD1 permits the degradation of ssDNA stretches removed from the stalled forks preventing accumulation of ssDNA in the cytosol and induction of the interferon response.[11]

Genetic defects in SAMHD1 cause human pathologies linked to either of the two recognized functions of the protein, that is, as a dNTP pool regulator and a defense against inflammatory response. Lack of the former function is considered to underlie several cancers by lowering the fidelity of DNA synthesis, lack of the latter to cause the congenital inflammatory Aicardi-Goutières Syndrome (AGS). The cellular consequences of SAMHD1 deficiency have been investigated by knocking down the protein by different approaches in normal or transformed cells. Loss of SAMHD1 is accompanied by expansion of the dNTP pools, particularly large in non-dividing cells. However, only in a minority of cases all four dNTPs have been examined, revealing that they undergo differential changes which result in pool imbalance. Purine dNTPs increased more than pyrimidine dNTPs in transformed cells,[12,13] in primary fibroblasts,[8] and in whole mouse embryos.[14] In elutriated SAMHD1-KO THP1 cells, all dNTP pools were expanded in all phases relative to parental SAMHD1-proficient cells, but purines increased more than pyrimidines in G1 and G2/M, whereas in S phase the fold-increase in dCTP was similar to those of dATP and dGTP.[10]

Besides the effects on dNTP pool composition, in normal human fibroblasts siRNA-silencing of SAMHD1 inhibits cell proliferation and disturbs the G1/S transition.[8] Similarly, in *S cerevisiae* the expansion of dNTP pools produced by overexpression of a RNR variant with altered allosteric regulation, transiently arrests cell cycle progression in late G1 phase delaying the activation of prereplicative complexes at the origins of replication.[15] In the case of transformed cells, the effects of SAMHD1 downregulation on cell cycle progression are controversial. Some studies reported reduced proliferation,[11,16] others accelerated growth,[13] and we did not find any significant difference relative to the controls.[10]

There is no in vivo evidence for anti-proliferative effects of SAMHD1 deficiency. Humans carrying germ-line mutations in SAMHD1 undergo normal development before manifesting AGS, often with a late onset presentation.[17] Moreover, the lack of SAMHD1 in mouse and zebrafish models did not perturb development.[18-20]

Pool imbalances have documented destabilizing effects, inducing misincorporation of the dNTP present in excess, interfering with correct chain elongation and causing structural alterations of chromosomes.[1,2,21-23] The abnormal dNTP pools associated with SAMHD1 deficiency may contribute to cancer development. SAMHD1 mutations were first recognized as potential founding events in chronic lymphocytic leukemias[24] and later identified in additional forms of leukemia[25] and in solid tumors.[14,26] On this basis, SAMHD1 was suggested to function as a tumor suppressor. Moreover, SAMHD1 deficiency may have a twofold influence on DNA repair. The induced imbalance of dNTP pools may affect the efficiency of DNA repair synthesis[27] and the recruitment of proteins involved in HR-mediated repair of DNA double-strand breaks may be impaired by the lack of SAMHD1.[28]

Considering the potential problems arising from the experimental suppression of SAMHD1 activity, here we chose to study the effects of an endogenous lack of SAMHD1 on cell proliferation and genomic stability in primary skin fibroblasts derived from four unrelated AGS patients carrying different SAMHD1 mutations.

2 | MATERIALS AND METHODS

2.1 | Cell lines

We used four lines of skin fibroblasts derived from patients affected by AGS with inactivating mutations in SAMHD1 (Prof. Y. Crow collection, University of Manchester, UK). Patient P1 (AGS282) is a compound heterozygote carrying mutations R145X and R164X,[29] patient P2 (AGS295) carried the homozygous deletion of exons 12-16,[30] patient P3 (AGS165) carried the homozygous nucleotide deletion 359-370,[31] and patient P4 (AGS128) carried the homozygous mutation Q149X.[31] Appropriate written informed consent was obtained from the parents of the patients for inclusion in this study, which was approved by the Leeds (East) Multi-Centre Research Ethics Committee. Three lines of age-matched control skin fibroblasts were available in our laboratory (WT1, WT2, and WT3). Human monocytic cells (THP1) knockout for SAMHD1 and matched control were donated by Prof. T. Gramberg.[32]

2.2 | Cell growth, cell cycle analysis, and SA-β-galactosidase staining

All fibroblasts were grown in DMEM with 4.5 g/L glucose, 10% (v/v) fetal calf serum (FCS), non-essential amino acids, and antibiotics. To ensure comparability in all experiments, cell cultures were used at similar passage numbers. THP1 cells were cultured in RPMI with 10% (v/v) FCS.

Cell cycle distribution was determined by flow cytometry after propidium iodide staining of fixed resuspended cells, with a FACSCanto II Flow cytometer (BD Biosciences, San Jose, CA, USA). To identify 20% S phase enriched cell cultures, sets of 0.2 million cells/10 cm dish were seeded and collected for FACS analysis between 30 and 48 hours after seeding every 2-3 hours.

To quantify the percentage of senescent cells, WT and AGS fibroblasts were seeded at 0.05 million cells/35 mm dish. After 48 hours, cells were fixed and stained using the senescence cells histochemical staining kit (Sigma Aldrich, St. Louis, MO, USA). To quantify the SA-β-Gal-positive cells > 700 cells were counted for each sample using several fields.

2.3 | Cumulative population doubling level

To evaluate replicative lifespan, cells of P1 and P2 and of two controls (WT1 and WT2) were serially subcultured every 4 days for 5 months, seeding 0.4 million cells in 75 cm^2 flasks. The daily population doublings numbers (PDN) were calculated by the formula {ln [(number of cells harvested)/(number of cells seeded)]/ln 2}/4 days and added to the previous PDNs to yield the cumulative PDN value.

2.4 | Western blotting

All procedures were performed as described in Franzolin et al (2015).[33] Samples of 1-2 million cells were collected by centrifugation, washed with PBS, and lysed with radioimmunoprecipitation assay buffer (10 mM TrisHCl pH 7.4, 100mM NaCl, 1% sodium deoxycholate, 0.1% SDS, 1% Nonidet P-40) containing a mixture of protease inhibitors for mammalian cells (Sigma Aldrich). The extracts were centrifuged at 19 000 *g* for 20 minutes, the protein concentrations of the supernatant solutions were determined by the Pierce BCA protein assay kit (Thermo Fisher Scientific, Waltham MA, USA), and 20 μg or 10 μg of the cleared supernatants, respectively, from proliferating and resting cells were loaded on precast gels 7.5% (Bio-Rad, Hercules, CA, USA) and electrophoresed. The proteins were blotted on Hybond-C extra (GE Healthcare, Chicago, IL, USA) and saturated with 2% non-fat milk (Euroclone) for 1 hour at room temperature and incubated overnight at 4°C with the primary anti-SAMHD1 antibody (1:4000, PROTEINTECH group, Rosemont, IL, USA) or anti-β actin (1:10 000, Sigma Aldrich). After 3 washings with PBS + 0.05% Tween 20 for 10 minutes, the membranes were incubated with horseradish peroxidase-conjugated secondary antibodies (1:40 000 and 1:100 000, respectively) for 1 hour at room temperature. Then the membranes were washed and developed with a chemiluminescence ECL kit (LiteAblotTurbo, Euroclone S.p.a, Pero, MI, Italy). The signals were detected on Kodak films.

2.5 | Quantitation of dNTP pools

Cycling cell cultures were obtained seeding 0.2 million cells/10 cm dish and were harvested after 32-48 hours growth. For confluent cell, cultures were seeded at 0.4 million cells/10 cm dish. At confluence, the medium was replaced with 0.1% FBS medium and cells were harvested after 10 days of quiescence with fresh 0.1% FCS medium being supplied twice weekly. Dishes were cooled on ice, the cells were carefully washed free of medium and extracted with ice-cold 60% methanol. After immersion for 3 minutes in a boiling water bath, the methanolic extract was centrifuged and brought to dryness by centrifugal evaporation. The dry residue was dissolved in 0.2 mL of water and used for assays. The four dNTPs were determined by an enzymatic assay modified as described in Ferraro et al (2010).[34]

2.6 | RNA extraction, reverse transcription, and quantitative real-time PCR (qRT-PCR)

RNA extraction, reverse transcription, and real-time PCR were done as described by Franzolin et al (2013).[8] TRIzol Reagent (Thermo Fisher Scientific) was used to extract RNA from cell cultures according to the manufacturer's protocol. Prior to RNA extraction, cell cultures were washed in PBS to remove excess medium then Trizol was added directly on the dish and cells were detached using a cell scraper. RNA quantity and quality was tested by UV spectrophotometry and with electrophoresis by 2100 Agilent Bioanalyzer (Agilent Technologies, Santa Clara, CA, USA) following the protocol provided by the manufacturer. We quantified by qRT-PCR with QuantiTect Primer assay kit (Qiagen, Hilden, Germany) the mRNA of SAMHD1, BRCA1, E2F2, CDT1, PRIM1, CDC7, MLH1 using as housekeeping gene Succinate Dehydrogenase Complex Flavoprotein Subunit A (SDHA). SAMHD1 primer which amplifies exons 1, 2, and 3 allowed us to detect SAMHD1 mRNA both in WT and AGS mutant fibroblasts with mutations localized in exons 4, 5, or in the C terminus.

2.7 | Microarray experiments and data analysis

Fluorescent cRNA to be hybridized onto microarrays was produced by Low Input Quick Amp Labeling Kit (Agilent Technologies) according to the manufacturer's instructions. Labeled cRNA was dispersed onto the microarray to perform the hybridization (65°C, 17 hours, 10 rpm rotation). Slides were washed using Wash Buffer Kit (Agilent Technologies) and dried at room temperature. Microarray slides were scanned using G2505C scanner (Agilent Technologies) at 3-μm resolution. Probe features were extracted using the Feature Extraction Software v. 10.7.3.1 with GE_1_Sep09 protocol (Agilent Technologies). Intra-array normalization was directly performed by the Feature Extraction Software. Raw and normalized data are available in the GEO database (GSE 135652). For each sample, we set probe expression to NA (not available) when flag "Positive and Significant" from Feature Extraction Software was "FALSE." To normalize data, we used quantile inter-arrays normalization (normalizeQuantiles, limma R package). Data for long non-coding RNAs were excluded for the normalization of coding RNAs. The expression of probes with the same ProbeName was averaged.

Microarray data were analyzed using the MultiExperiment Viewer (MeV, Ver. 4.8).[35] We used a *t* test (from MeV) to identify differentially expressed RNAs between cells derived from AGS patients and WT. *P* values were computed using a gene permutation approach and corrected using Bonferroni. We consider a gene differentially expressed when the corrected *P* value was $\leq .05$. Differentially expressed genes resulting from each comparison were grouped to identify interesting profiles considering all samples. Gene grouping was performed using the Self Organizing Tree Algorithm (SOTA)[36] implemented in the MultiExperiment Viewer software. Clustering was performed using the Pearson correlation. Genes in specific clusters were classified according to their function using the Reactome database implemented in the WEB-based GEne SeT AnaLysis Toolkit.[37] The Benjamini and Hochberg correction for multiple tests was used to calculate FDR corresponding to each pathway.

2.8 | UV irradiation of cells and analysis of photoproducts

Cell monolayers were irradiated with a 254-nm UVS-11 mineral light lamp at a fluency rate of 2 J/m^2/sec. Then fresh medium was added, and the cells were returned to culture conditions for the indicated time points. Genomic DNA was isolated using the Puregene Core Kit B (Qiagen). Dot blot immunoassays were performed to determine the relative amounts of UV-induced photoproducts CPDs and 6-4PPs in total genomic DNA from cells collected at different times after UV irradiation, as described in Pontarin et al (2012).[27] All experiments were performed in duplicate. The relative intensity of each signal was determined using ImageJ program.

2.9 | Fluorometric analysis of DNA unwinding

Fluorometric analysis of DNA unwinding (FADU) was performed 30, 60, 90, and 180 minutes after UV irradiation with 24 J/m^2 following the protocol described in Pontarin et al (2012).[27]

To avoid DNA resynthesis after UV damage, in a parallel experiment cells were maintained in the presence of 12 μM aphidicolin (APH) and added to the medium 1 hour before UV irradiation and maintained until harvesting.

2.10 | Clonogenic cell survival assay

0.2 million cells were seeded in 10 cm plates and 3 days later were irradiated with 0-6-12-18-24-30 J/m^2 of UV light. To calculate the percent survival, 100 not irradiated cells, 300 cells irradiated with 6 and 12 J/m^2, 500 cells treated with 18 and 24 J/m^2, or 1000 cells irradiated with 30 J/m^2 were spread on 5 cm diameter plates (10 plates for each dose of UV light). Cells were grown at 37°C for 15 days and the number of

viable colonies was counted. The colony number from the non-irradiated control plates was averaged and taken as 100% viability.

2.11 | NGS library preparation, sequencing, and data analysis

0.4 million cells/10 cm dish were seeded in 10% FBS medium. When confluence was reached cells were treated with 5 nM AllStar negative control siRNA (catalog no.1027281 Qiagen) or with siRNA anti-MLH1 (catalog no. SI00005404 Qiagen) in medium containing 0.1% FBS. The cells were transfected using 1 μL RNAiMAX (LifeTechnologies, Carlsbad, CA, USA)/mL of medium. After 4 days, the cells were treated again with siRNA as before and after 2 days genomic DNA (gDNA) was extracted with the Puregene Core Kit B (Qiagen). At the same time point, MLH1 expression was assessed by qRT-PCR. All siCTRL samples had similar MLH1 mRNA levels and silencing left 20%-30% residual level of mRNA.

The Qubit DNA HS assay kit (Thermo Fisher Scientific) was used to quantify purified gDNA. DNA libraries were prepared using reagents provided in the TruSeq Exome Library Prep Kit (Illumina, San Diego, CA, USA) following the manufacturer's instructions. Briefly, 100 ng of input gDNA was sonicated with Covaris S2 machine and fragment distribution was checked on 2100 Agilent Bioanalyzer using a High Sensitivity DNA chip (Agilent Technologies). Afterwards, a 10-cycles PCR step was performed using unique single 6 base index adapters on the P7 strand to generate barcoded libraries. For the enrichment, two hybridizations were carried out using capture probes according to the manufacturer's protocols. Then the enriched libraries were amplified and quantified with Qubit fluorometer using a dsDNA HS kit (Thermo Fisher Scientific). The size distribution of post-enriched libraries was checked using the 2100 Agilent Bioanalyzer DNA High sensitivity assay (Agilent Technologies). A 75bp paired-end sequencing was performed on Illumina NextSeq500 using the NextSeq500 High Output Kit v2 (150 cycles). The following samples were independently sequenced to obtain four biological replicates of each condition (WT si-CTRL, WT si-MLH1, P si-CTRL, and P si-MLH1). A total of 16 samples were thus sequenced. Due to poor sequencing quality, one WT si-CTRL specimen was discarded from the analysis. FASTQ files were processed according to the GATK best practices (https://www.broadinstitute.org/partnerships/education/broade/best-practices-variant-calling-gatk-1). In particular, 75 bp paired-end reads were aligned on the primary assembly of the hg19 reference genome using BWA mem (v. 0.7.12 with default parameters)[38] and the resulting BAM files[39] were marked for optical and PCR duplicates (Picard MarkDuplicatesWithMateCigar v2.3.0), corrected for misalignment around indels and recalibrated for the base quality score (GATK BaseQualityScoreRecalibrator v3.6-0). The mean coverage of the samples treated with control siRNA was planned to be near 120X, as they were designed to be used as references in the subsequent analysis, while the other samples should reach a value of 30X. Somatic variant calling was performed using VarDict[40] in the paired mode. The set of aligned reads of each sample was sub-sampled, taking points at 1, 2, 5, 7, and 10 millions randomly collected reads. At least three technical replicates were taken for each point, not allowing the same read to occur more than once at each point. The resulting variants were selected to keep only single nucleotide variants (SNVs) with base quality > 30, covered by just a single mutated read in the sub-sample and none in the control. This procedure should select only very recently occurring mutations, while the probability of discarding two or more variants falling at the same position remains negligible. On the other hand, it must be considered that true mutations and sequencing errors cannot be distinguished at this stage; therefore, we refer to these variants as mismatches. Mismatches were plotted as a function of the read number to create tendency lines whose slope should be proportional to the mismatch frequency of the sample. Thus, mismatch frequency is calculated by dividing the slope of tendency line by the read length (75 bp). This value corresponds to the sum of de novo mutation frequency which depends on sample experimental conditions and intrinsic sequencing error frequency that are expected to be similar among the samples. The mean of the mismatches related to each technical replica was used to perform a statistical comparison of the various biological conditions. Regression slopes were calculated by the Ordinary Least Squares (OLS) model and evaluated by the StatsModels Python Library, whereas the comparison of the data at the middle of the regressions (5 million reads) was evaluated by Tukey's HSD test.

2.12 | Molecular combing and genome-wide DNA replication analysis

Sub-confluent AGS (P1 and P2) and WT (WT1 and WT2) fibroblasts as well as exponentially growing SAMHD1-KO and WT THP1 cells were labeled with sequential 30 minutes pulses of 50 μM 5-Iodo-2′-deoxyuridine (IdU; Sigma-Aldrich) and 100 μM 5-Chloro-2′-deoxyuridine (CldU; Sigma-Aldrich), respectively. When cells were exposed to replication stress (0.4 μM APH for 2 hours), labeling was performed during the last hour of APH treatment. 1-2x10^5 cells were immobilized in agarose plugs and incubated overnight at 50°C in 2 mg/mL Proteinase K solution (1% N-laurosylsarcosine, 0.1 M EDTA pH 8.0, 0.01 M Tris-HCl pH 8.0, 0.02 M NaCl). After digestion with β-agarase I (New England BioLabs, Ipswich, MA, USA), high molecular

weight DNA from 1-2 plugs was delivered in 0.1 M MES pH 6.1. DNA combing was performed on silanized surfaces according to a standard procedure and well-established criteria of analysis.[41-43] Briefly, genome-wide replication analysis was carried out by IdU and CldU immunodetection, and the integrity of the DNA molecules was assessed by an anti-ssDNA antibody. A motorized fluorescence microscope (Zeiss Axio Imager.M1) equipped with a CCD camera (Photometrix, Coolsnap HQ2) was used for microscope analyses. Adobe Photoshop CS2 and Metavue Research Imaging System (Molecular Devices, San Jose, CA, USA) software were used for image analyses. A complete description can be found in Refs. [41,42]. Replication rates were calculated considering complete bidirectional forks only. All other patterns, including forks with unidirectional progression and possible deregulation events, such as asynchronous and paused/arrested forks, were recorded. Replication cluster length and DNA molecule length were also determined. The latter represents the control for quality/integrity of combed DNA.

2.13 | Statistical analysis

Statistical analyses were performed with either parametric or non-parametric tests, according to data distribution of each experimental setting. Details are given in the table and figure legends.

3 | RESULTS

3.1 | The dNTP pools of AGS fibroblasts are strongly increased and severely imbalanced

SAMHD1 silencing in non-transformed human skin and lung fibroblasts results in increased and imbalanced dNTP pools.[8] Similar dNTP pool changes were reported in KO mice constitutively deficient for SAMHD1,[18] whereas dNTP pools in SAMHD1-deficient patients cells have not been carefully investigated. We studied four lines of human skin fibroblasts isolated from unrelated AGS patients (P1 to 4) with inactivating mutations of SAMHD1.[29-31] We first compared the expression of SAMHD1 mRNA during proliferation in AGS and WT (WT1 and WT2) fibroblasts. The mRNA level was comparable in WT, P3 and P4 cells, but about 90% lower in P1 and P2 cells (Supplemental Table S1). Whereas in WT fibroblasts, the concentration of the SAMHD1 protein was higher in quiescent than in cycling cells, as reported previously,[8] in the SAMHD1-mutated lines the protein was undetectable, independently of mRNA expression and growth conditions (Supplemental Figure S1).

Next, we measured the four dNTP pools in cycling and quiescent cultures of WT and AGS cells (Figure 1A,B) and calculated the percentage of each dNTP in the total pool (Figure 1C,D). To compare the unsynchronized proliferating cultures and the dNTP concentrations that depend on the frequency of S phase cells, we used cultures with the same percentage of S phase cells (20% in Figure 1A,C). In all AGS lines, each of the four dNTP pools was increased, but to different extents (Figure 1A). Purine pools were increased much more than pyrimidine pools. The dGTP pool was 5-15 times higher in AGS than in WT fibroblasts ($P < .001$), followed by dATP, three- to sixfold expanded ($P < .001$). The increase in pyrimidine deoxynucleotides was modest, dTTP was 2-4 times higher in AGS cells ($P < .001$) whereas dCTP, roughly doubled in P3 and P4 fibroblasts ($P < .01$), was only marginally increased in P1 and P2 cells (Figure 1A). Similar dNTP pool changes were observed previously in siRNA-silenced skin fibroblasts.[8] The differences among the four AGS lines may be ascribed to inter-individual variability in the expression of synthetic and catabolic enzymes involved in deoxynucleotide metabolism.[33]

To estimate to which extent SAMHD1 is involved in dNTP pool regulation during quiescence, we compared dNTP pool sizes in serum-starved cultures (max 1%-2% S phase cells). Under those conditions, the absence of SAMHD1 favored a remarkable expansion of dNTP pools (Figure 1B). In AGS fibroblasts, both dGTP and dATP were 50- to 200-fold higher than in WT cells ($P < .01$), whereas pyrimidine dNTPs increased much less, dTTP 6- to 10-fold and dCTP threefold only in P3 and P4 cells ($P < .01$). Surprisingly, in resting AGS cells, purine dNTPs were two orders of magnitude higher than in quiescent skin fibroblasts siRNA-silenced for SAMHD1.[8] These data point to a major role of SAMHD1 in setting dNTP pool balance outside S phase.

In normal skin fibroblasts, purine dNTPs make up 25%-30% of the total dNTP content independently of the proliferation state.[34] The same occurred here in the WT fibroblasts (Figure 1C,D), whereas in AGS fibroblasts dNTP pool composition was markedly altered ($P < .001$). During proliferation, purine dNTPs amounted to 50% of the total pool and up to 80% during quiescence (Figure 1C,D). Indeed, an impressive common feature of the AGS lines was their huge pool imbalance. In spite of some variability in pool expansion, a chi square analysis showed that the relative frequency of each dNTP in the total pool was similar in all mutants ($P < .001$) (Figure 1C,D). We wondered which consequences such unusual dNTP pools may have for cell proliferation and genome stability.

3.2 | SAMHD1-deficient fibroblasts can adapt to high dNTP content and grow normally

Considering the growth-inhibitory effects described earlier in normal cells devoid of SAMHD1 activity, we asked

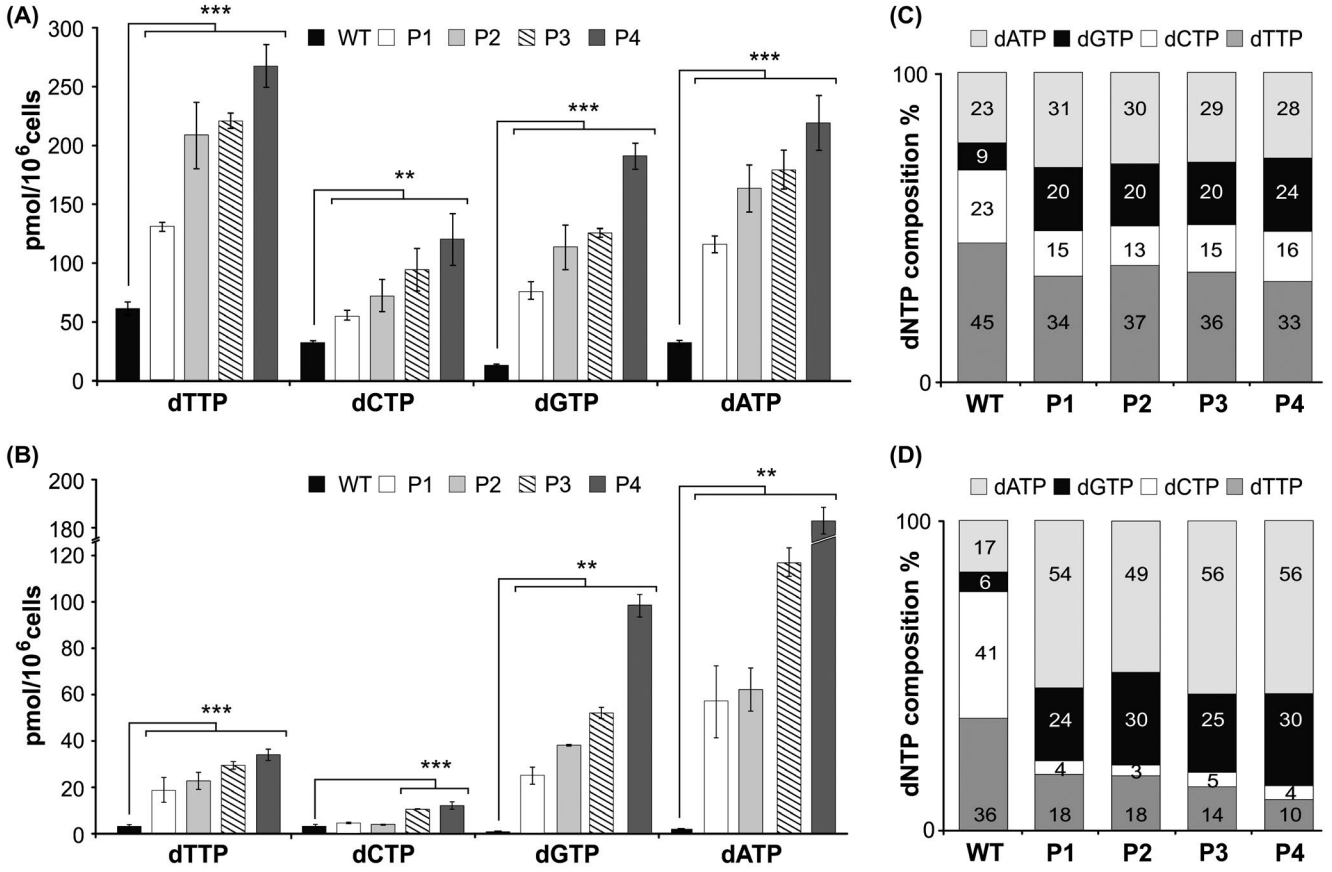

FIGURE 1 dNTP cellular sizes and composition in AGS and WT skin fibroblasts. dNTP pool sizes were measured in cycling cell cultures with 20% S phase cells (A) and in quiescent cultures maintained for 10 days in 0.1% FCS serum (B). Data are means ± SE from at least four experiments for each cell line. Statistical analysis was performed using a two-tailed *t* test, $^{**}P < .01$, $^{***}P < .001$. To evaluate the balance of the dNTP pool, we calculated the relative percentage abundance of each dNTP in the total pool in proliferating (C) and quiescent samples (D). The values of two WT cell lines (WT1 and WT2) were averaged, whereas those of the patient lines (P1, P2, P3 and P4) are reported separately

whether the chronic dNTP pool imbalance of the four AGS cell lines examined here interfered with their cell cycle progression. The individual lines behaved differently: P3 and P4 cells grew poorly similar to the AGS skin fibroblasts studied by Kretschmer and coworkers,[44] whereas P1 cells grew like the controls and P2 cells, although slow-growing, reached the stationary phase at a WT cell density (Figure 2A). We estimated the degree of senescence in AGS and WT cell cultures at early[10-15] and late[30-40] passages after isolation (Figure 2B). Populations of P3 and P4 cells became senescent at early passages and contained 40% and 60% SA-β-Gal stained cells, respectively. The senescent plateau was associated with cell flattening and increase in SA-β-Gal-positive cells. Conversely, AGS P1 and P2 cells reached senescence after about 50 population doublings like the WT fibroblasts (Figure 2C).

We hypothesized that the growth differences among the AGS lines might be linked to different gene expression, resulting in a different capacity to cope with dNTP pool imbalance. To obtain a global view of the transcriptional changes in the SAMHD1 mutants relative to WT fibroblasts, we performed a genome-wide RNA expression analysis. The RNA samples were prepared from asynchronous populations with 20% S phase cells. The analysis of gene set enrichment profiles did not reveal any significant interferon-related signature, in contrast to a previous report.[44] However, some genes induced by interferon were overexpressed in P1 and P2 cells relative to WT fibroblasts, for example, the interferon alpha inducible protein 27 (IFI27) gene (8 times in P1 and 62 times in P2) and interferon-induced protein 44 like (IFI44L) gene (6 times in P1 and 15 times in P2) (Supplemental Figure S2). Differentially expressed genes were grouped into 11 clusters according to their expression profiles to identify genes with shared profiles (Figure 3A and Supplemental Data S1). Cluster 1 includes genes activated only in P3 and P4 cells, cluster 10 includes genes downregulated in P3 and P4 cells, and clusters 5 and 6 group genes activated only in P1 and P2 cells (Supplemental Data S2). Cluster 1 was enriched for genes belonging to pathways associated with senescence such as the oxidative stress–induced senescence pathway or the SIRT1-associated pathway. Clusters 5, 6,

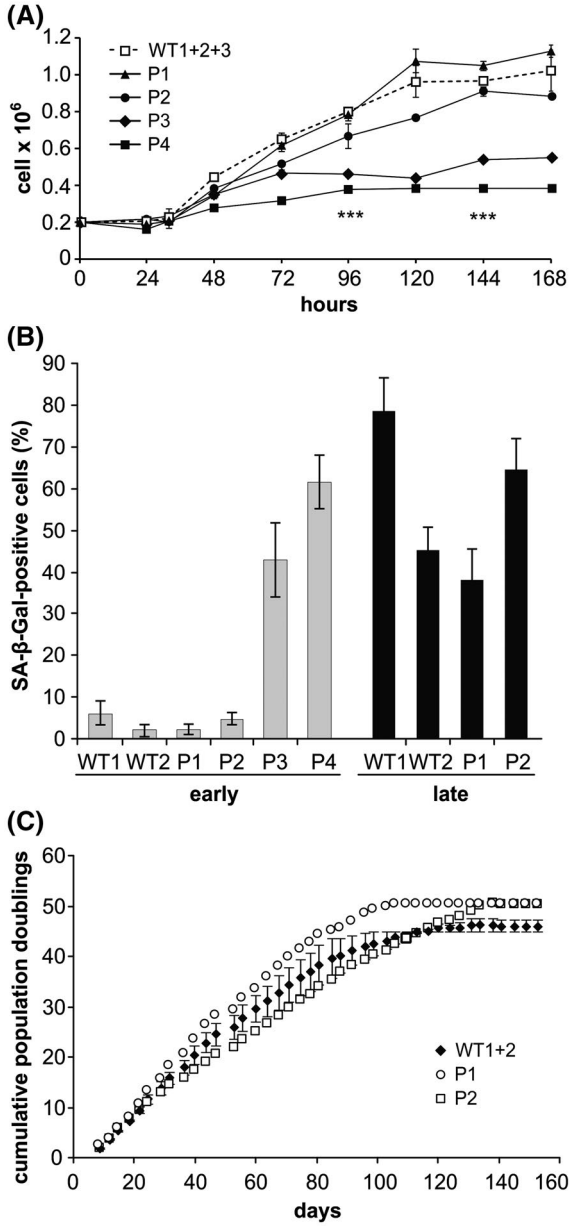

FIGURE 2 SAMHD1-deficient fibroblasts enter senescence prematurely or adapt to high dNTP content growing normally. A, Time-dependent growth in culture of AGS mutant (P1, P2, P3 and P4) and control (WT) cells from early passages. The values of three WT cell line (WT1 + WT2 + WT3) were averaged. Data are means ± SE from three experiments for each cell line. Statistical significance of differences between the group of WT, P1 and P2 with the group of P3 and P4 fibroblast lines was compared with *t* test at 96 and 144 hours of growth, ***$P < .001$. B, Percentage of SA-β-galactosidase-positive cells in two WT cell lines (WT1 and WT2) and in the four AGS fibroblast lines (P1, P2, P3, and P4) at early passages (8-20 passages) and at late passages (30-50 passages). At least 700 cells were counted in each condition. The values are expressed as mean ± SD. C, Cumulative population doubling curves of WT and AGS P1 and P2 fibroblasts. The values of two WT cell lines (WT1 and WT2) were averaged and error bars represent the range of values, whereas those of the patient lines (P1, P2) are reported separately. Viable cells were counted every 4 days for 5 months

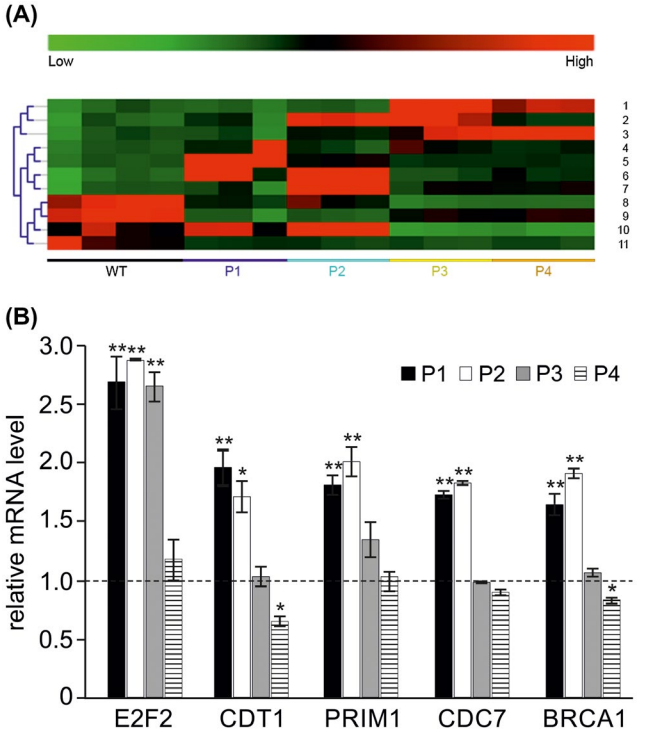

FIGURE 3 Heat map of differentially expressed genes in control (WT1) and AGS (P1, P2, P3, P4) skin fibroblasts and validation by qRT-PCR. A, Differentially expressed genes were grouped into 11 clusters according to their expression profiles. Green, low expression; red, high expression. Three or four biological replicates were tested for each AGS and WT line, respectively. B, Validation of mRNA microarray results for five annotated genes of clusters 5 and 6. qRT PCR was run on RNA from samples with 20% S phase cells. The level of expression of each RNA is compared with that of WT1. Data are means ± SE of three biological replicates each analyzed in triplicate. The statistical significance between each AGS (P1, P2, P3, and P4) and WT fibroblast line was calculated by a two-tailed *t* test. *$P < .05$, **$P < .001$

and 10 were enriched for genes involved in DNA replication and cell cycle progression, clusters 5 and 6 being in addition enriched for genes of DNA repair pathways (Table 1 and Supplemental Data S3). Microarray results were validated by qRT-PCR for five genes from clusters 5 and 6 (Figure 3B and Supplemental Figure S3). The correlation among microarray and qRT-PCR data varied between 75% and 95% (Supplemental Figure S3). The E2F2 transcription factor active at the G1/S transition was upregulated almost threefold in P1, P2, and P3 samples (Figure 3B). CDT1, coding for an essential licensing protein and PRIM1 and CDC7, also required for DNA replication, were almost twofold upregulated in P1 and P2 cells only. Similarly upregulated was BRCA1 which, besides its function in DNA repair, has a role in replication fork stability.[45] Our analysis suggests that some cell lines, like the present P1 and P2 fibroblasts, can adapt to SAMHD1 deficiency and the resulting abnormal dNTP pools by upregulation of genes

TABLE 1 Pathway enrichment analysis of specific gene clusters identified from differentially expressed genes in SAMHD1-deficient fibroblasts

Pathway[a]	
Cluster 1[b]	**FDR**[c]
Packaging of telomere ends	3.96 e^{-03}
SIRT1 negatively regulates rRNA expression	4.67 e^{-03}
Oxidative stress–induced senescence	4.67 e^{-03}
Cluster 10[b]	
Cell cycle	1.3 e^{-02}
Cell cycle, mitotic	1.55 e^{-02}
Cluster 5 and 6[b]	
Cell cycle	6.49 e^{-12}
DNA repair	8.25 e^{-05}
Cell cycle checkpoints	1.65 e^{-04}

[a]Pathway names were derived from Reactome database.

[b]Clusters in Figure 3A.

[c]False Discovery Rate (FDR) was calculated using the Benjamini and Hochberg correction for multiple tests.

involved in G1/S transition and DNA replication. In contrast, other SAMHD1 mutants fail to adapt and enter a premature senescent state. Considering the poor proliferation ability of the P3 and P4 lines, we continued our study with the P1 and P2 AGS lines.

3.3 | DNA replication dynamics is unaffected in AGS fibroblasts but altered in a SAMHD1-KO transformed cell line

An insufficient supply of dNTPs causes global slowdown of replication fork speed and increased origin firing by activation of the DNA damage response.[46-49] The effect on replication dynamics produced by an excess of DNA precursors remains to be assessed. In yeast, a moderate increase in dNTP levels protected cells from replication stress and promoted replication fork progression.[50] In human cells, SAMHD1 deficiency with the associated strong dNTP pool expansion may affect per se DNA replication dynamics.

To address this question, we analyzed replication dynamics in AGS P1 and P2 fibroblasts and WT1 and WT2 fibroblasts. No differences in terms of fork progression rate, inter origin distance (IOD), and cluster size were observed among the four cell lines (Figure 4A-D and Supplemental Table S2). Furthermore, the same frequencies of unidirectional forks and pause/arrest events were observed in all samples (Supplemental Table S2) and fell within the ranges observed in other mammalian cells.[51,52] To investigate whether the large dNTP pools modify the tolerance of AGS cells to replication stress, as reported in yeast,[50] replication profiles of P2 and WT1 fibroblasts were assessed after treatment with aphidicolin (APH, 0.4 μM). As expected due to the inhibitory effect of APH on DNA replication, a significant reduction of fork rates, IOD and cluster size were observed in comparison to untreated samples, but no differential response was found between APH-treated P2 and WT1 cells (Figure 4A-D and Supplemental Table S2). Upon reduction of the replication cluster size, the frequency of firing origins increased in both AGS and WT fibroblasts compared to untreated cells ($P < .001$) (Figure 4E, Supplemental Table S2), again with no difference between mutant and WT cells. Importantly, the distribution of molecule length was consistent among all samples and was not affected from APH treatment (Figure 4D), allowing to exclude that the cluster size reduction induced by APH was an artifact related to the quality of combed DNA molecules. Finally, no differential response to APH emerged also considering the additional replication parameters (unidirectional, paused/arrested, asynchronous forks) (Supplemental Table S2). Taken together, these data show that AGS P1 and P2 fibroblasts preserve normal DNA replication dynamics.

We had already found that SAMHD1 knockout in THP1 cells (a transformed monocytic cell line) expanded DNA precursor pools,[10] with some differences compared to the present AGS fibroblasts. In SAMHD1-KO THP1 cells, the largest pool was dATP and the dTTP pool was minimally changed (Supplemental Figure S4). The lack of SAMHD1 increased the percent abundance of purine dNTPs in the pool from 8% to 23% but the total pool still consisted largely of pyrimidine dNTPs, that in SAMHD1-proficient THP1 cells represented 92% of the pool (Supplemental Figure S4). In parental and SAMHD1-KO THP1 cells, the analysis of replication dynamics highlighted a pronounced reduction ($P < .001$) in fork rates, IOD, and cluster size in THP1-KO cells (Figure 4A-D and Supplemental Table S2). In addition, the number of activated origins per cluster was significantly increased ($P < .001$) relative to the parental THP1 cell line (Figure 4F and Supplemental Table S2). This feature may account for the ability of the SAMHD1-KO THP1 cells to proliferate at the same rate as the parental THP1 cells.[10] Finally, the proportion of paused/arrested forks was doubled in THP1-KO, although the difference with the parental cells lacked statistical significance (Supplemental Table S2). On the whole, the replication dynamics observed in THP1 cells deficient for SAMHD1 points to an endogenous replication stress.

The observed differences in DNA replication dynamics between untransformed AGS fibroblasts and transformed SAMHD1-KO THP1 cells may result from intrinsic differences between cell types and/or development of an adaptive phenotype in AGS cells. The latter hypothesis is supported by the gene expression profiles differentiating AGS P1 and P2 cell lines from WT fibroblasts.

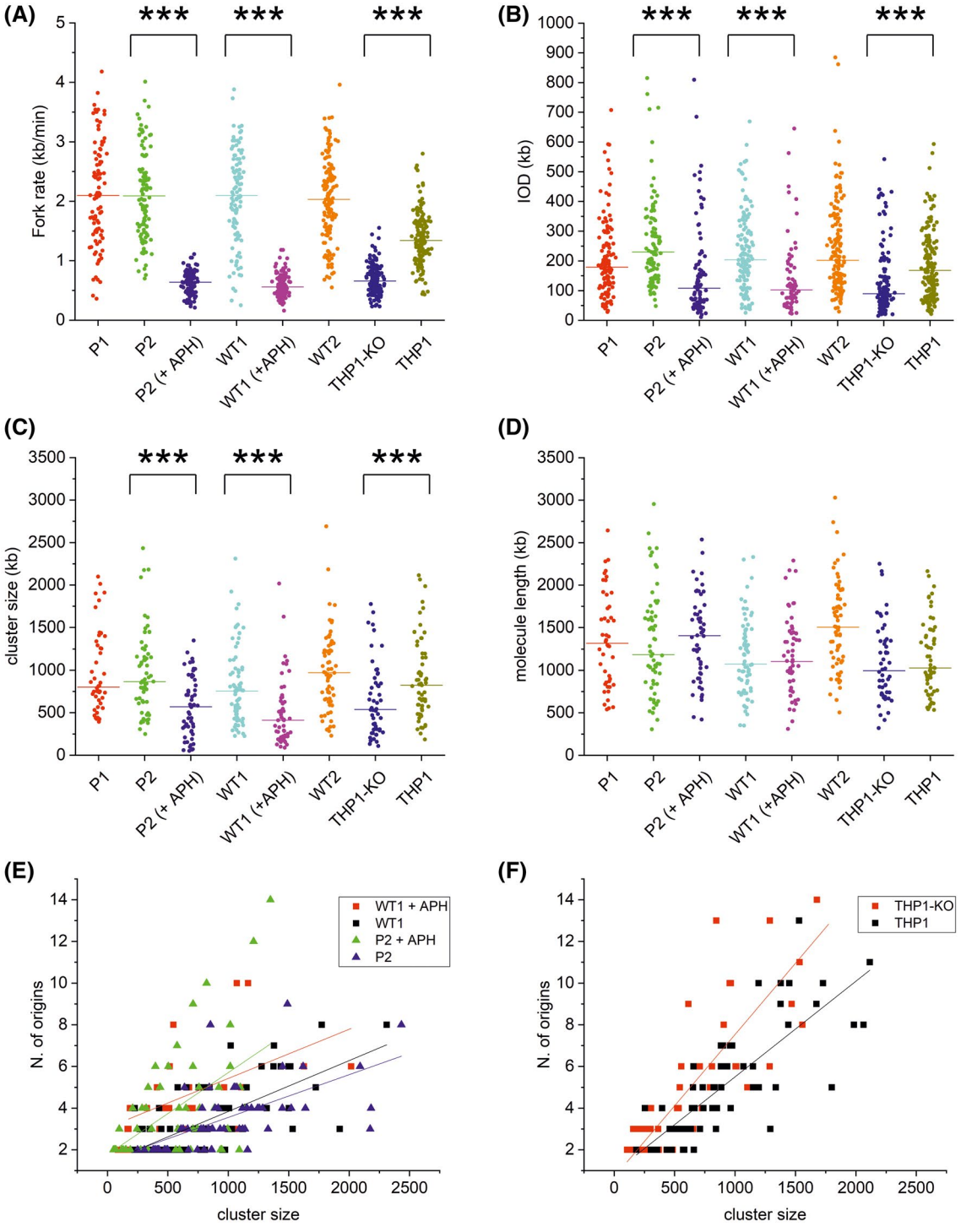

FIGURE 4 Replication dynamics of SAMHD1-deficient cells. Distributions of fork rates (A), inter-origin distances, IOD (B), cluster size (C), molecule lengths (D) in AGS mutant cells (P1, P2) compared to WT fibroblasts (WT1, WT2) and in THP1-KO compared to THP1 cells. P2 and WT1 fibroblasts were analyzed also after APH-induced replication stress. ***$P < .001$, Kruskal-Wallis non-parametric test. Color lines represent the median of each distribution. E, Number of activated origins as a function of cluster size in P2 (blue symbols, untreated; green symbols, APH-treated) and WT1 (black symbols, untreated; red symbols, APH-treated) cells. A significant increase in origin firing was detected for both cell types after APH-induced replication stress ($P < .001$ for the comparison between regression slopes), whereas untreated SAMHD1-deficient and WT fibroblasts did not differ. F, Number of activated origins as a function of cluster size in THP1-KO (SAMHD1-deficient, red symbols) and THP1 (black symbols) cells. All the samples fit a linear regression model ($P < .001$). The *b* values of the two regression lines are significantly different ($P < .001$) indicating that SAMHD1-deficient cells activate a higher number of origins per cluster than WT THP1 cells. Datasets are shown in Supplemental Table S2

3.4 | The aberrant dNTP content of SAMHD1-deficient cells increases their mutation frequency

Minor alterations of dNTP pools increase the mutation frequencies of colon cancer cells lacking a functional mismatch repair.[14] To assess whether the aberrant dNTP pool composition in P1 and P2 fibroblasts is mutagenic for these non-transformed cells, we designed an approach based on next-generation sequencing (NGS). The DNA was extracted from AGS (P1 and P2) and WT (WT1 and 2) fibroblasts treated for 6 days with control siRNA (si-CTRL) or with a siRNA targeting the mismatch repair gene MLH1 (si-MLH1), to amplify the potential mutagenicity of the high dNTP pools.

For a quantitative comparison of mismatch frequencies between AGS and WT fibroblasts, we focused on exome sequences and built by high coverage (120X) whole exome sequencing (WES) a reference sequence for each of the four cell lines treated with control siRNA. Sequencing errors intrinsic to NGS technology might overshadow the de novo mutations generated by imbalanced dNTP pools or MLH1 silencing. To minimize this problem, we considered only bases with Phred quality score >30 (probability of error smaller than 1/1250) and only single nucleotide variants (SNVs) referred as mismatches. A detailed description of the procedure is reported in Material and Methods. Figure 5 summarizes our results showing the number of mismatches in each sample plotted as a function of read number. We performed two independent silencing experiments for all cell lines and conditions of treatment. Data from WT1 and WT2 samples were combined as well as those from P1 and P2 samples. Considering the experimental design, the slope of the tendency lines is expected to be proportional to the mismatch frequency of each sample, that is, the sum of de novo mutation frequency and intrinsic sequencing error frequency. WT fibroblasts treated with si-CTRL (WT si-CTRL) showed the lowest mismatch frequency that we considered essentially equal to that of the sequencing errors. As the read length was 75 bases, the calculated mismatch frequency in WT si-CTRL samples was about 1.1/10 000 bp which is lower than expected with a Q value > 30. Most importantly, the accuracy of the measurements was very high, with a very contained sampling error, thus permitting to detect small differences of mismatch frequencies among samples.

With MLH1 silencing, WT cells presented an increased mismatch frequency (1.39/10 000 bp), comparable to that of AGS fibroblasts treated with control siRNA (P si-CTRL) (1.37/10 000 bp). This result indicates that SAMHD1 deficiency is associated with an accumulation of genomic mutations even when MLH1-dependent repair is functional. MLH1 silencing in AGS fibroblasts further increased the frequency of mismatches to 1.56/10 000 bp. Assuming that all samples were affected by the same sequencing error frequency and using as baseline the mismatches found in WT cells (light blue line in Figure 5), we estimated the mutation frequencies of the other samples, that is, 0.29/10 000 bp in

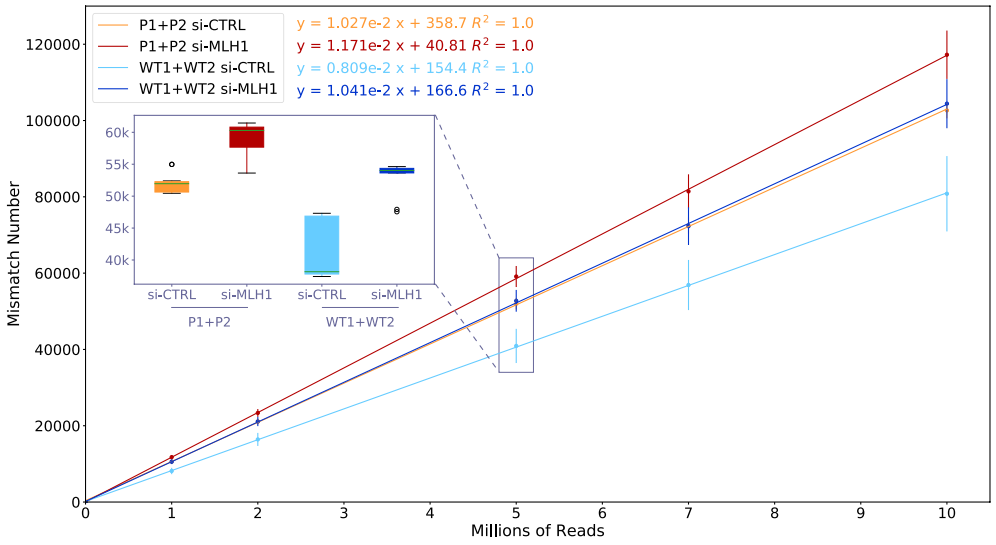

FIGURE 5 Mismatch quantitation by NGS analysis. The number of mismatches detected in SAMHD1-WT (WT1 + WT2) and AGS fibroblasts (P1 + P2) treated for 6 days with non-target siRNA (si-CTRL) or MLH1-siRNA (si-MLH1) is plotted against the number of analyzed reads. All samples were analyzed with NGS in two independent silencing experiments to have for each cell line two different sequencing runs. These data were used to build tendency lines by linear regression, whose equations are shown on the top. WT1 + WT2 si-CTRL tendency line (light-blue), mainly due to sequencing errors, constitutes the baseline for comparisons with the other samples. Linear regressions of P1 + P2 si-CTRL, P1 + P2 si-MLH1, and WT1 + WT2 si-MLH1 are represented in gold, red, and blue, respectively. Boxplots are used to explore sample mismatch at 5 million (5M) reads. The results of statistical analysis are summarized in Supplemental Table S3

MLH1-silenced WT, 0.27/10 000 bp in AGS si-CTRL, and 0.46/10 000 bp in MLH1-silenced AGS cells.

To estimate the significance of the observed differences, we performed two parallel statistical analyses. Briefly, the first method compared the slopes of the regression lines, whereas the second compared the number of variants at 5 million reads (Figure 5 and Supplemental Table S3). We found for WT si-CTRL samples (WT1 + WT2) a slope significantly lower than all the others. Moreover, the slope of the AGS si-CTRL samples (P1 + P2) was significantly lower than that of the MLH1-silenced AGS samples (P1 + P2 si-MLH1) ($P = 3.55e{-}05$) but similar to MLH1-silenced WT ($P = .696$). The results obtained at 5 million reads confirmed the differences observed by slope analysis, but in this case the comparisons between P1 + P2 si-MLH1 against either WT si-MLH1 or P1 + P2 si-CTRL do not reach significant probability values (Supplemental Table S3).

These data support the hypothesis that SAMHD1 deficiency and/or the related imbalanced dNTP pool may be per se a mutagenic condition that promotes genome instability in non-transformed cells.

3.5 | Faster nucleotide excision repair after UV damage in quiescent SAMHD1-deficient fibroblasts

Nucleotide excision repair (NER) removes bulky DNA lesions such as those caused by UV light. The resynthesis step requires dNTPs to fill the gaps arising from excision of the UV-induced photoproducts, after which DNA ligases seal the nicks and restore the original dsDNA. NER is the repair mechanism requiring the highest amount of dNTPs and should be most sensitive to deviations of dNTP concentrations from their physiological level. In fact, when the supply of one or more dNTPs is limited, for example, in quiescent p53R2-mutated human fibroblasts, NER is delayed.[27] We asked whether the opposite condition, that is, increased supply of dNTPs, affects NER dynamics and examined the ability of the AGS mutant fibroblasts to repair DNA after UV irradiation. We first tested the clonogenic cell survival of cycling AGS and WT fibroblasts after increasing doses of UV-C. Both P1 and P2 cells were less sensitive to UV-induced lethality than WT fibroblasts at each irradiation dose (Figure 6A). The exposure resulted in 90% cell killing after 12 J/m^2 for WT cell lines and 18 J/m^2 for P1 and P2 mutants. To study NER efficiency, we employed quiescent cultures on account of the very large expansion of dNTP pools in quiescent AGS versus WT fibroblasts (see above) and because repair assays based on measurements of NER-mediated DNA breaks are more sensitive in G0/G1 phase.[53] After 10 days of incubation in 0.1% FCS, cell cultures were irradiated with 24 J/m^2 UV-C, a dose that under quiescence is not lethal.[27]

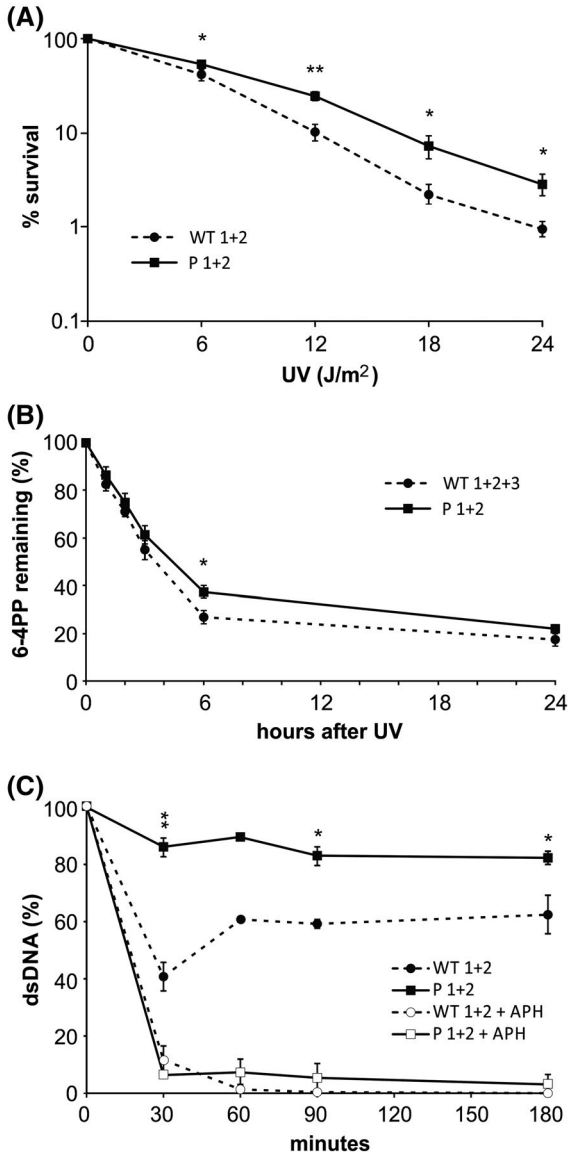

FIGURE 6 DNA repair in UV-irradiated AGS mutant and WT fibroblasts. A, Clonogenic survival in two AGS mutant (P1 + P2) and two control (WT1 + WT2) fibroblast lines after UV-C irradiation. The experiment was repeated at least twice for each cell line and bars indicate SE of the mean. B, Disappearance of primary DNA damage in AGS mutant (P1 + P2) and control (WT1 + WT2 + WT3) fibroblasts. We irradiated quiescent cells with 24 J/m^2 UV light and used specific monoclonal antibodies to identify the disappearance of 6-4 PPs over the subsequent 24 hours. Values are means of three different experiments performed in duplicate for each cell line and bars indicate SE of the means. C, Time course of DNA repair in quiescent AGS mutant (P1 + P2) and control fibroblasts (WT1 + WT2) lines after irradiation with UV (24 J/m^2) in the presence or absence of aphidicolin (APH). The fraction of intact dsDNA relative to not irradiated samples was measured by FADU from the fluorescence of EtBr bound to alkali-treated DNA. Values are means of at least three different experiments for each cell line in absence of APH and of two experiments for each cell line in the presence of 12 μM APH. Bars indicate SE. Statistical significance for the differences between AGS and WT fibroblasts was calculated by two-tailed *t* test (*$P < .05$, **$P < .001$), the significance shown in (C) refers to the comparison between samples not treated with APH

Using specific antibodies, we determined the time-dependent disappearance of the two main UV-induced photoproducts, cyclobutane pyrimidine dimers (CPDs) and 6-4 pyrimidone photo-products (6-4PPs). After irradiation, 50% of the 6-4PPs was removed during the first 6 hours, in agreement with previous reports,[27] similarly in WT and AGS cells (Figure 6B). As expected, CPD removal took considerably longer. After 24 hours, the damages were reduced only by 30% in both WT and AGS fibroblasts (data not shown). These results indicate that the early recognition and removal of the damaged sites occurred with similar efficiency in SAMHD1-mutant and WT cells.

Then we studied the gap-filling step measuring rejoining of the repair-induced DNA strand breaks by fluorometric analysis of DNA unwinding (FADU) after EtBr staining.[27] Before the ligation step, alkali treatment of the nicked DNA produces single-stranded regions at the sites of initial damage. The ongoing DNA repair is monitored measuring the EtBr-fluorescence of the DNA remaining double stranded after alkaline incubation. Quiescent WT and AGS fibroblasts irradiated with 24 J/m^2 UV-C were allowed to repair their DNA for up to 3 hours in conditioned medium in the presence or absence of aphidicolin (12 μM), added 1 hour before irradiation. DNA strand break production in WT and AGS fibroblasts was the same when the resynthesis step was inhibited by APH during repair incubation, suggesting that the irradiation had caused the same level of damage in both types of cells (Figure 6C). Conversely, in the absence of APH, the SAMHD1-mutant cell lines recovered double-stranded DNA faster than the WT cells (90% vs 50% dsDNA at 30 minutes from irradiation; $P < .001$) (Figure 6C). Taken together, these experiments suggest that the strong dNTP pool expansion caused by SAMHD1 inactivity stimulates the rate of single strand gap filling by DNA polymerases improving the overall rate of the repair process.

4 | DISCUSSION

The gene coding for SAMHD1 was described in the year 2000,[54] but the interest in the protein began to soar only a decade later, following the discoveries about its multiple biological functions and its implications for human health. SAMHD1 was found to act as host restriction factor against HIV1 and other lentiviruses[55] on account of its enzyme activity as a dNTP triphosphohydrolase.[56,57] Moreover, loss of function of the gene was associated with the Aicardi-Goutières Syndrome[31] and cancer.[24] Early studies employed transformed human cells in culture to investigate the effects of SAMHD1 knockdown on the dNTP pools and/or HIV1 replication.[55] In a previous study, we employed non-transformed human fibroblasts silenced by siRNA transfections. That approach provided a clear demonstration of the major role of SAMHD1 in keeping dNTP pool balance during the cell cycle and in quiescence.[8] Here, we extend our investigation to cells constitutively devoid of SAMHD1 activity to assess how normal human fibroblasts react to a constitutive alteration of dNTP pool composition and if the chronic pool imbalance affects their genetic stability. The only similar study published so far employed AGS skin fibroblasts isolated from two patients carrying SAMHD1 mutations different from those of the present patients and measured the dATP and dGTP pools only.[44]

The dNTP pool alterations found here in the four AGS lines were even more striking than those observed earlier in SAMHD1-silenced fibroblasts.[8] Despite some variability in pool sizes, the changes in pool composition were remarkably similar in the four lines, providing a general picture of the pool changes produced by SAMHD1 deficiency. The main feature is the large increase in purine dNTPs, in agreement with earlier reports.[8,12-14] Notably, the dGTP pool, normally the smallest[34,58] undergoes the largest expansion in the absence of SAMHD1 (Figure 1). This increase was previously ascribed to the fact that dGTP is the best substrate for the purified enzyme, on the basis of its K_M.[6,59] However, the K_M differences for the four dNTPs are relatively small and the two purines, dGTP and dATP, lie at the two extremes of the K_M range. We suggest that the larger increase in purine dNTPs reflects not only the loss of SAMHD1 catabolic activity but also the modulation of the anabolic activity of RNR by its allosteric effectors (Figure 7). The increased concentration of dTTP stimulates GDP reduction by RNR favoring accumulation of dGTP that, in turn, stimulates ADP reduction to dADP and inhibits reduction of pyrimidine nucleotides.[7] Thus, lack of SAMHD1 influences dNTP de novo synthesis by changing the concentrations of the allosteric effectors active at the substrate specificity site of RNR. The increase in dATP, that works as negative effector at RNR activity site,[7] clearly does not shut down dNTP synthesis completely.

An additional factor for the specific accumulation of dGTP and dATP is the different composition of the enzyme network regulating purine vs pyrimidine dNTPs. The catabolism of deoxyguanosine and deoxyadenosine released from dGTP and dATP by SAMHD1 is performed by purine nucleoside phosphorylase (PNP) and adenosine deaminase (ADA).[4,60] These two enzymes are more widely expressed and more active in vivo than the corresponding phosphorylase and deaminase degrading thymidine and deoxycytidine (reviewed in 4). Degradation of the two purine deoxynucleosides lowers their probability to be directly recycled to deoxynucleotides by the relevant deoxynucleoside kinases (Figure 7). In SAMHD1-proficient cells, the fast removal of purine compounds from the dNTP pool is likely balanced by an optimized rate of de novo synthesis by RNR. With the loss of SAMHD1, the whole catabolic component of the regulatory network loses its impact, as

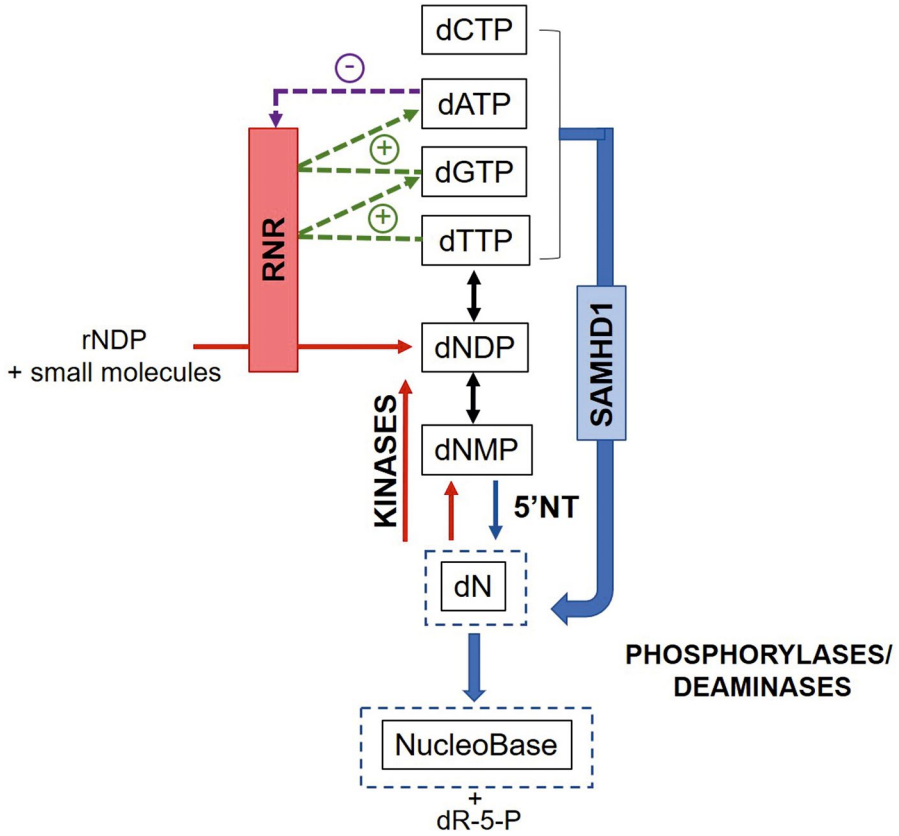

FIGURE 7 Enzymatic network for dNTP synthesis and degradation in mammalian cells. dNTP pool composition is regulated by synthetic and catabolic enzymes. dNTPs are mainly synthesized by de novo synthesis in the cytosol by ribonucleotide reductase (RNR) or through the salvage of deoxynucleosides (dN) by deoxynucleoside kinases. RNR activity is allosterically regulated: once formed, dTTP promotes the reduction of GDP to dGDP favoring the accumulation of dGTP which, in turn, inhibits reduction of pyrimidine ribonucleosides. Conversely, dGTP induces the reduction of ADP to dADP. High concentrations of dATP inhibit the overall activity of RNR. The two synthetic pathways are counteracted by catabolic activities. In the nucleus, SAMHD1 degrades dNTPs to the corresponding deoxynucleosides (dN) which are also produced in the cytosol or in the mitochondria by 5′-nucleotidases (5′NT). dN are either exchanged across the plasma membrane by equilibrative transporters or further degraded by nucleoside phosphorylases and deaminases to free nucleobases that are diffusible across the plasma membrane. Green dashed lines indicate stimulation of RNR activity, purple dashed lines indicate inhibition. Blue dashed lines highlight metabolites able to cross the plasma membrane

PNP and ADA are deprived of the major part of their deoxynucleoside substrates normally produced by SAMHD1. As a consequence, the anabolic component of the network prevails, boosting the purine dNTP pools. The weight of this mechanism for the expansion of the dGTP and dATP pools may vary, depending on the expression of PNP and ADA in the individual cells and tissues.

When active, SAMHD1 transforms plasma membrane-impermeable dNTPs into deoxynucleosides that are transferred bidirectionally across the membrane by equilibrative transporters[61] following the concentration gradients. In this way, the cell can adjust its dNTP concentrations to the conditions of its microenvironment. In the absence of SAMHD1, production of deoxynucleosides relies exclusively on 5′-nucleotidases, that, judging from the effects of their loss or gain of function,[62,63] in vivo are much less active than SAMHD1.

We had earlier reported that in human fibroblasts the expansion of the dNTP pools after SAMHD1 silencing quickly inhibited cell proliferation, leading to accumulation of cells in G0 within 48-72 hours. This block of the cell cycle conflicts with the basically normal development of human patients and animal models of SAMHD1 deficiency.[18-20] In the four AGS lines studied here, we observed two different patterns of growth in vitro, namely normal proliferation or precocious senescence (Figure 2), connected to different gene expression patterns. The P1 and P2 lines, growing similar to WT fibroblasts, revealed slightly (2-3 fold) increased expression of key genes controlling cell cycle progression and DNA replication (Figure 3), suggesting that such a small overexpression suffices to preserve normal proliferation in non-transformed cells. We propose that some genetic backgrounds favor the upregulation of pro-growth genes permitting normal cell proliferation, whereas cells more prone to

upregulate pro-senescence genes grow slowly and manifest an early senescent phenotype.

The dNTP pools in SAMHD1-mutated fibroblasts are characterized by a marked imbalance deriving from uneven expansion of the individual dNTPs. Imbalanced dNTP pools are known to cause replication stress and impair the cell ability to preserve its genetic information.[1,2,21,22] Indeed, a newly described function of SAMHD1 is exerted at stalled replication forks during the replication stress response.[11] To investigate the consequences of SAMHD1 deficiency for the genomic stability of AGS fibroblasts, we examined three critical features, the dynamics of DNA replication, the rate of UV-induced DNA repair, and the overall fidelity of DNA synthesis. Our data show that, in contrast to what occurs in transformed cell lines when SAMHD1 is experimentally inactivated (Figure 4 and 11), the non-senescent SAMHD1-deficient fibroblasts uphold normal DNA replication dynamics despite the concomitant dNTP pool imbalance. This difference may depend on the altered cell cycle control of the transformed cells and suggests that the modest variations of pro-growth gene expression in AGS cells support their control of S phase progression.

In quiescent cells, after UV damage, the large pools associated with lack of SAMHD1 favor the resynthesis step of NER (Figure 6C), leaving the previous detection and removal of the photoproducts unchanged compared to WT fibroblasts (Figure 6B). The dependence of NER resynthesis on the availability of dNTPs in non-cycling cells is highlighted by the comparison between the present AGS fibroblasts and the p53R2-deficient fibroblasts reported earlier,[27] where the low pools associated with impaired de novo synthesis delayed the final steps of NER.

Thus, SAMHD1-deficient human fibroblasts can synthesize DNA efficiently both during replication and repair, but how faithful is their DNA synthesis? Their large and imbalanced dNTP pools are expected to reduce the fidelity of DNA polymerases by interfering with their selectivity and proofreading activity[23,58] and by favoring mismatch extension.[23] The mutagenic consequences of the pool alterations produced by total or partial SAMHD1 loss of function have been reported earlier in colon-rectal carcinoma cells.[14] Here, we found a similar situation even in non-cancer cells. Remarkably, the absence of SAMHD1 in AGS fibroblasts (P1 + P2 si-CTRL) led to the same frequency of mismatches as the inactivation of MMR in SAMHD1-proficient controls (WT1 + WT2 si-MLH1) (Figure 5 and Supplemental Table S3). Downregulation of MLH1 in AGS cells resulted in almost twofold increase in the mutation frequency. Our data are in strict agreement with a different study where mutation frequencies were compared in MLH1-deficient cancer cells with or without increased dNTP pools to mimic SAMHD1 deficiency.[14] The high mutation frequency in SAMHD1-deficient fibroblasts is likely related to the nature of their pool imbalance, that is, enlarged pools with very high dGTP, similar to the most mutagenic imbalance described by Schmidt et al.[58] On this basis, we cannot exclude that an accumulation of somatic mutations in AGS cells may have contributed to the ability of P1 and P2 fibroblasts to proliferate in culture.

SAMHD1 was proposed to act as a tumor suppressor, controlling the size and balance of the four dNTPs and contributing to the fidelity of DNA synthesis.[24] In agreement with this view, our findings indicate that SAMHD1 deficiency is per se sufficient to elicit a mutator phenotype in non-transformed cells. Similar to genes of DNA repair pathways, SAMHD1 can be classified as a caretaker of genome stability.

ACKNOWLEDGMENT

We thank Prof. Y. Crow (Manchester Centre for Genomic Medicine, University of Manchester, Manchester, United Kingdom) for kindly providing the AGS cell lines and Prof. T. Gramberg (Institute of Clinical and Molecular Virology, Friedrich-Alexander University Erlangen-Nürnberg, Erlangen, Germany) for the THP-1 lines used in this study.

CONFLICT OF INTEREST

None declared.

AUTHOR CONTRIBUTIONS

E. Franzolin, V. Bianchi, and C. Rampazzo designed the study; E. Franzolin, S. Coletta, and C. Rampazzo performed cell cycle analyses, SA-β-galactosidase staining experiments, western blot, dNTP pool quantitation, UV irradiation experiments, and clonogenic cell survival assay; E. Franzolin and C. Rampazzo performed and analyzed qRT-PCR data and MLH1 silencing experiments; E. Franzolin, S. Coletta, P. Ferraro, and G. D'Aronco performed and analyzed FADU experiments; G. Pontarin measured photoproducts; M. Stevanoni, E. Palumbo, and A. Russo designed and performed DNA combing experiments; S. Cagnin performed and analyzed Microarray experiments; L. Bertoldi, E. Feltrin, and G. Valle performed and analyzed next-generation sequencing experiments; V. Bianchi and C. Rampazzo wrote the manuscript and all authors reviewed and accepted it.

DATA AVAILABILITY STATEMENT

Microarray data were submitted to Gene Expression Omnibus (GEO) database: GSE135652. NGS genomic data were submitted to Sequence Read Archive (SRA) database: PRJNA558189.

REFERENCES

1. Meuth M, L'Heureux-Huard N, Trudel M. Characterization of a mutator gene in Chinese hamster ovary cells. *Proc Natl Acad Sci U S A*. 1979;76:6505-6509.
2. Weinberg G, Ullman B, Martin DW Jr. Mutator phenotypes in mammalian cell mutants with distinct biochemical defects and

abnormal deoxyribonucleoside triphosphate pools. *Proc Natl Acad Sci U S A*. 1981;78:2447-2451.
3. Reichard P. Interactions between deoxyribonucleotide and DNA synthesis. *Annu Rev Biochem*. 1988;57:349-374.
4. Rampazzo C, Miazzi C, Franzolin E, et al. Regulation by degradation, a cellular defense against deoxyribonucleotide pool imbalances. *Mutat Res Genet Toxicol Environ Mutagen*. 2010;703:2-10.
5. Pontarin G, Ferraro P, Hakansson P, Thelander L, Reichard P, Bianchi V. p53R2-dependent ribonucleotide reduction provides deoxyribonucleotides in quiescent human fibroblasts in the absence of induced DNA damage. *J Biol Chem*. 2007;282:16820-16828.
6. Ji X, Tang C, Zhao Q, Wang W, Xiong Y. Structural basis of cellular dNTP regulation by SAMHD1. *Proc Natl Acad Sci U S A*. 2014;111:E4305-E4314.
7. Nordlund P, Reichard P. Ribonucleotide reductases. *Annu Rev Biochem*. 2006;75:681-706.
8. Franzolin E, Pontarin G, Rampazzo C, et al. The deoxynucleotide triphosphohydrolase SAMHD1 is a major regulator of DNA precursor pools in mammalian cells. *Proc Natl Acad Sci U S A*. 2013;110:14272-14277.
9. Tang C, Ji X, Wu L, Xiong Y. Impaired dNTPase activity of SAMHD1 by phosphomimetic mutation of Thr-592. *J Biol Chem*. 2015;290:26352-26359.
10. Tramentozzi E, Ferraro P, Hossain M, Stillman B, Bianchi V, Pontarin G. The dNTP triphosphohydrolase activity of SAMHD1 persists during S-phase when the enzyme is phosphorylated at T592. *Cell Cycle*. 2018;17:1102-1114.
11. Coquel F, Silva M-J, Técher H, et al. SAMHD1 acts at stalled replication forks to prevent interferon induction. *Nature*. 2018;557:57-61.
12. Nguyen LA, Kim DH, Daly MB, Allan KC, Kim B. Host SAMHD1 protein promotes HIV-1 recombination in macrophages. *J Biol Chem*. 2014;289:2489-2496.
13. Bonifati S, Daly MB, St. Gelais C, et al. SAMHD1 controls cell cycle status, apoptosis and HIV-1 infection in monocytic THP-1 cells. *Virology*. 2016;495:92-100.
14. Rentoft M, Lindell K, Tran P, et al. Heterozygous colon cancer-associated mutations of SAMHD1 have functional significance. *Proc Natl Acad Sci U S A*. 2016;113:4723-4728.
15. Chabes A, Stillman B. Constitutively high dNTP concentration inhibits cell cycle progression and the DNA damage checkpoint in yeast Saccharomyces cerevisiae. *Proc Natl Acad Sci U S A*. 2007;104:1183-1188.
16. Lee EJ, Seo JH, Park J-H, et al. SAMHD1 acetylation enhances its deoxynucleotide triphosphohydrolase activity and promotes cancer cell proliferation. *Oncotarget*. 2017;8:68517-68529.
17. Crow YJ. Aicardi-Goutières syndrome. *Handb Clin Neurol*. 2013;113:1629-1635.
18. Rehwinkel J, Maelfait J, Bridgeman A, et al. SAMHD1-dependent retroviral control and escape in mice. *EMBO J*. 2013;32:2454-2462.
19. Behrendt R, Schumann T, Gerbaulet A, et al. Mouse SAMHD1 has antiretroviral activity and suppresses a spontaneous cell-intrinsic antiviral response. *Cell Rep*. 2013;4:689-696.
20. Kasher PR, Jenkinson EM, Briolat V, et al. Characterization of *samhd1* morphant zebrafish recapitulates features of the human type I interferonopathy Aicardi-Goutières syndrome. *J Immunol*. 2015;194:2819-2825.
21. Kunkel TA. DNA replication fidelity. *J Biol Chem*. 1992;267:18251-18254.
22. Kumar D, Abdulovic AL, Viberg J, Nilsson AK, Kunkel TA, Chabes A. Mechanisms of mutagenesis in vivo due to imbalanced dNTP pools. *Nucleic Acids Res*. 2011;39:1360-1371.
23. Watt DL, Buckland RJ, Lujan SA, Kunkel TA, Chabes A. Genome-wide analysis of the specificity and mechanisms of replication infidelity driven by imbalanced dNTP pools. *Nucleic Acids Res*. 2015;44:1669-1680.
24. Clifford R, Louis T, Robbe P, et al. SAMHD1 is mutated recurrently in chronic lymphocytic leukemia and is involved in response to DNA damage. *Blood*. 2014;123:1021-1031.
25. Johansson P, Klein-Hitpass L, Choidas A, et al. SAMHD1 is recurrently mutated in T-cell prolymphocytic leukemia. *Blood Cancer J*. 2018;8:11.
26. Wang JL, Lu FZ, Shen XY, Wu Y, Zhao LT. SAMHD1 is down regulated in lung cancer by methylation and inhibits tumor cell proliferation. *Biochem Biophys Res Commun*. 2014;455:229-233.
27. Pontarin G, Ferraro P, Bee L, Reichard P, Bianchi V. Mammalian ribonucleotide reductase subunit p53R2 is required for mitochondrial DNA replication and DNA repair in quiescent cells. *Proc Natl Acad Sci U S A*. 2012;109:13302-13307.
28. Daddacha W, Koyen AE, Bastien AJ, et al. SAMHD1 promotes DNA end resection to facilitate DNA repair by homologous recombination. *Cell Rep*. 2017;20:1921-1935.
29. Rice GI, Forte GMA, Szynkiewicz M, et al. Assessment of interferon-related biomarkers in Aicardi-Goutières syndrome associated with mutations in TREX1, RNASEH2A, RNASEH2B, RNASEH2C, SAMHD1, and ADAR: a case-control study. *Lancet Neurol*. 2013;12:1159-1169.
30. Ramesh V, Bernardi B, Stafa A, et al. Intracerebral large artery disease in Aicardi-Goutières syndrome implicates SAMHD1 in vascular homeostasis. *Dev Med Child Neurol*. 2010;52:725-732.
31. Rice GI, Bond J, Asipu A, et al. Mutations involved in Aicardi-Goutieres syndrome implicate SAMHD1 as regulator of the innate immune response. *Nat Genet*. 2009;41:829-832.
32. Wittmann S, Behrendt R, Eissmann K, et al. Phosphorylation of murine SAMHD1 regulates its antiretroviral activity. *Retrovirology*. 2015;12:103.
33. Franzolin E, Salata C, Bianchi V, Rampazzo C. The deoxynucleoside triphosphate triphosphohydrolase activity of SAMHD1 protein contributes to the mitochondrial DNA depletion associated with genetic deficiency of deoxyguanosine kinase. *J Biol Chem*. 2015;290:25986-25996.
34. Ferraro P, Franzolin E, Pontarin G, Reichard P, Bianchi V. Quantitation of cellular deoxynucleoside triphosphates. *Nucleic Acids Res*. 2010;38:e85.
35. Saeed AI, Sharov V, White J, et al. TM4: a free, open-source system for microarray data management and analysis. *Biotechniques*. 2003;34:374-378.
36. Herrero J, Valencia A, Dopazo J. A hierarchical unsupervised growing neural network for clustering gene expression patterns. *Bioinformatics*. 2001;17:126-136.
37. Wang J, Vasaikar S, Shi Z, Greer M, Zhang B. WebGestalt 2017: a more comprehensive, powerful, flexible and interactive gene set enrichment analysis toolkit. *Nucleic Acids Res*. 2017;45:W130-W137.
38. Li H, Durbin R. Fast and accurate long-read alignment with Burrows-Wheeler transform. *Bioinformatics*. 2010;26:589-595.
39. Li H, Handsaker B, Wysoker A, et al. The Sequence Alignment/Map format and SAMtools. *Bioinformatics*. 2009;25:2078-2079.

40. Lai Z, Markovets A, Ahdesmaki M, et al. VarDict: a novel and versatile variant caller for next-generation sequencing in cancer research. *Nucleic Acids Res*. 2016;44:e108.
41. Palumbo E, Matricardi L, Tosoni E, Bensimon A, Russo A. Replication dynamics at common fragile site FRA6E. *Chromosoma*. 2010;119:575-587.
42. Palumbo E, Tosoni E, Russo A. General and specific replication profiles are detected in normal human cells by genome-wide and single-locus molecular combing. *Exp Cell Res*. 2013;319:3081-3093.
43. Conti C, Saccà B, Herrick J, Lalou C, Pommier Y, Bensimon A. Replication fork velocities at adjacent replication origins are coordinately modified during DNA replication in human cells. *Mol Biol Cell*. 2007;18:3059-3067.
44. Kretschmer S, Wolf C, König N, et al. SAMHD1 prevents autoimmunity by maintaining genome stability. *Ann Rheum Dis*. 2015;74:e17.
45. Kolinjivadi AM, Sannino V, de Antoni A, Técher H, Baldi G, Costanzo V. Moonlighting at replication forks—a new life for homologous recombination proteins BRCA1, BRCA2 and RAD51. *FEBS Lett*. 2017;591:1083-1100.
46. Kumar D, Viberg J, Nilsson AK, Chabes A. Highly mutagenic and severely imbalanced dNTP pools can escape detection by the S-phase checkpoint. *Nucleic Acids Res*. 2010;38:3975-3983.
47. Bester AC, Roniger M, Oren YS, et al. Nucleotide deficiency promotes genomic instability in early stages of cancer development. *Cell*. 2011;145:435-446.
48. Courbet S, Gay S, Arnoult N, et al. Replication fork movement sets chromatin loop size and origin choice in mammalian cells. *Nature*. 2008;455:557-560.
49. Anglana M, Apiou F, Bensimon A, Debatisse M. Dynamics of DNA replication in mammalian somatic cells: nucleotide pool modulates origin choice and interorigin spacing. *Cell*. 2003;114:385-394.
50. Poli J, Tsaponina O, Crabbé L, et al. dNTP pools determine fork progression and origin usage under replication stress. *EMBO J*. 2012;31:883-894.
51. Palumbo E, Tosoni E, Matricardi L, Russo A. Genetic instability of the tumor suppressor gene FHIT in normal human cells. *Genes Chromosomes Cancer*. 2013;52:832-844.
52. Stevanoni M, Palumbo E, Russo A. The replication of frataxin gene is assured by activation of dormant origins in the presence of a GAA-repeat expansion. *PLOS Genet*. 2016;12:e1006201.
53. Thyagarajan B, Anderson KE, Lessard CJ, et al. Alkaline unwinding flow cytometry assay to measure nucleotide excision repair. *Mutagenesis*. 2007;22:147-153.
54. Li N, Zhang W, Cao X. Identification of human homologue of mouse IFN-gamma induced protein from human dendritic cells. *Immunol Lett*. 2000;74:221-224.
55. Laguette N, Sobhian B, Casartelli N, et al. SAMHD1 is the dendritic- and myeloid-cell-specific HIV-1 restriction factor counteracted by Vpx. *Nature*. 2011;474:654-657.
56. Goldstone DC, Ennis-Adeniran V, Hedden JJ, et al. HIV-1 restriction factor SAMHD1 is a deoxynucleoside triphosphate triphosphohydrolase. *Nature*. 2011;480:379-382.
57. Powell RD, Holland PJ, Hollis T, Perrino FW. Aicardi-Goutieres syndrome gene and HIV-1 restriction factor SAMHD1 is a dGTP-regulated deoxynucleotide triphosphohydrolase. *J Biol Chem*. 2011;286:43596-43600.
58. Schmidt TT, Sharma S, Reyes GX, et al. A genetic screen pinpoints ribonucleotide reductase residues that sustain dNTP homeostasis and specifies a highly mutagenic type of dNTP imbalance. *Nucleic Acids Res*. 2019;47:237-252.
59. Miazzi C, Ferraro P, Pontarin G, Rampazzo C, Reichard P, Bianchi V. Allosteric regulation of the human and mouse deoxyribonucleotide triphosphohydrolase sterile α-motif/histidine-aspartate domain-containing protein 1 (SAMHD1). *J Biol Chem*. 2014;289:18339-18346.
60. Goday A, Simmonds HA, Morris GS, Fairbanks LD. B cells as well as T cells form deoxynucleotides from either deoxyadenosine or deoxyguanosine. *Clin Exp Immunol*. 1984;56:39-48.
61. Baldwin SA, Beal PR, Yao SY, King AE, Cass CE, Young JD. The equilibrative nucleoside transporter family, SLC29. *Pflugers Arch*. 2004;447:735-743.
62. Rampazzo C, Ferraro P, Pontarin G, Fabris S, Reichard P, Bianchi V. Mitochondrial deoxyribonucleotides, pool sizes, synthesis, and regulation. *J Biol Chem*. 2004;279:17019-17026.
63. Gazziola C, Ferraro P, Moras M, Reichard P, Bianchi V. Cytosolic high K(m) 5′-nucleotidase and 5′(3′)-deoxyribonucleotidase in substrate cycles involved in nucleotide metabolism. *J Biol Chem*. 2001;276:6185-6190.

SUPPORTING INFORMATION

Additional supporting information may be found online in the Supporting Information section.

How to cite this article: Franzolin E, Coletta S, Ferraro P, et al. SAMHD1-deficient fibroblasts from Aicardi-Goutières Syndrome patients can escape senescence and accumulate mutations. *The FASEB Journal*. 2019;00:1–17. https://doi.org/10.1096/fj.201902508R